

Structural behavior of seawater sea-sand concrete shear wall reinforced with GFRP bars

Qingtian Zhang^a, Jianzhuang Xiao^{a,b,*}, Qingxiang Liao^a, Zhenhua Duan^a

^a Department of Structural Engineering, Tongji University, Shanghai 200092, China

^b Key Laboratory of Performance Evolution and Control for Engineering Structures, Ministry of Education, Tongji University, Shanghai 200092, China

ARTICLE INFO

Keywords:

Seawater sea-sand concrete (SSC)
Glass fiber reinforced plastic (GFRP)
Shear wall
Cyclic load
Seismic performance

ABSTRACT

This paper investigates the seismic performance of seawater sea-sand concrete (SSC) shear wall reinforced with glass fiber reinforced plastic (GFRP) bars. Three shear wall specimens were designed for the seismic performance evaluation, including natural aggregate concrete (NAC) reinforced with steel bars (SNW), NAC reinforced with GFRP bars (GNW) and SSC reinforced with GFRP bars (GSW). The results show that the application of SSC seems to have a negligible effect on the seismic performance of shear wall in the short term. The GNW and GSW have similar failure patterns and shapes of hysteresis curves. Also, with the same reinforcement ratio, the bearing capacity of GFRP reinforced specimens can be over 85% that of SNW while the deformability can reach the lateral drift up to 1/50. The ductility of GFRP reinforced specimen is lower than that of steel reinforced specimen but its residual deformation is relatively smaller. Furthermore, the applicability of existing design methods on the SSC shear wall is also evaluated.

1. Introduction

The conventional concrete is generally considered as unsustainable due to its massive consumption of natural resources and deterioration of the environment. According to the statistics [1], a numerous amount of raw materials was consumed in the past years due to the large-scale construction of concrete structures, which also led to substantial amount emissions of CO₂ [2,3]. In particular, a severe contradiction between supply and demand of raw materials can be noticed in some regions lacking in natural resource [4], especially for those areas around the marine and coast. The construction of concrete structures in such areas relies heavily on the long-distance transport of gravel, river sand and even freshwater, which increase the cost and energy consumption overall. On the contrary, the resources of seawater and sea-sand are locally and abundant, so the application of seawater sea-sand concrete (SSC) is recommended for the marine and coastal projects [5]. However, the use of SSC is still limited. The shell content of sea-sand is generally higher than that of river sand, which may influence the mechanical properties of concrete. Yang et al. [6] found that when oyster shells were used to replace 20% of the fine aggregate, the long-term strength of concrete was about 11.6% lower than that of ordinary concrete with the elastic modulus reduced by 10–15%. Also, due to the presence of high content of chloride in seawater and sea-sand, the steel reinforcement may be easily suffered from corrosion and thus

negatively affect the long-term performance of reinforced concrete structures [7,8]. To solve the problems related to corrosion, various methods have been suggested [9,10], such as adding corrosion inhibitors or applying functional coatings. The use of fiber reinforced plastic (FRP) as the reinforcement of SSC structures is a more effective method that can be regarded as an attractive and alternative option [11] since FRP have high chloride penetration resistance. Therefore, combined with FRP material, the seawater and sea-sand may be used in concrete without pre-treatment.

Due to the excellent malleability of FRP, it can be processed into sheets, plates, rods or tubes, which can be used as reinforcement or concrete confinement. Effective stress transfer between the FRP and concrete is essential, and the bond behavior is the fundamental problem to ensure the better performances of structures. Lu et al. [12] proposed some bond-slip models for FRP sheets/plates bonded to concrete to guide the design of FRP-strengthened reinforced concrete (RC) structures. Bond-slip between GFRP tube and concrete was proved to have little effect on the seismic behavior of GFRP tube columns [13]. Bond behavior of FRP bars depends on their mechanical properties and different surface configurations. Barris et al. [14] studied the influence of bond between FRP bar and concrete on crack width, and adjusted the bond coefficient for different existing formulations regarding crack spacing and crack width for FRP RC flexural elements. Based on these bond behavior research, there were several experimental studies on the

* Corresponding author at: Department of Structural Engineering, Tongji University, Shanghai 200092, China.

E-mail address: jzx@tongji.edu.cn (J. Xiao).

<https://doi.org/10.1016/j.engstruct.2019.03.101>

Received 3 November 2018; Received in revised form 27 March 2019; Accepted 27 March 2019

Available online 02 April 2019

0141-0296/ © 2019 Elsevier Ltd. All rights reserved.

FRP confined or reinforced concrete components. The limited effect of FRP by keeping fiber orientation in the transverse direction of the column can increase the compressive behavior of concrete columns [15]. Moreover, Qasrawi et al. [16] found that the localized damage decreased in FRP-confined concrete columns compared with that in conventional reinforced concrete columns under blast loading. As for the reinforced concrete, the FRP bars can be an alternative for steel bars. The GFRP bars reinforced beams showed typical bilinear behavior for strain and deflection until failure [17]. The ductility index of GFRP bars reinforced circular columns was 1.32–2.99 [18]. The shear capacity of beams reinforced by CFRP grid improved by 30–40% than that of ordinary steel reinforced concrete [19]. The combined use of FRP bars and PVA fiber concrete was also proved to be applicable and partial interaction model was proposed by Xie et al. [20] to guide the design for the composite beam. Also, an innovative closed-type winding GFRP stirrup was proposed by Dong et al. [21] in the concrete columns, and it improved the ductility of columns. All the results demonstrated the feasibility of using the FRP bars as reinforcement, and they can be used in variety ways. Besides, some specifications such as ACI 440.1R-15 [22] and GB 50608-2010 [23] were published to guide the design and construction of FRP reinforced concrete structures with river sand and fresh water. For the application of FRP bars in sea-sand based concrete, this idea was first proposed by Zha et al. [24]. It turned out to be a beneficial combination, as the FRP bars have high resistance against aggressive environments, the abundant resources of seawater and sea-sand can be directly used in producing concrete. Besides, due to the light weight of FRP bars, the cost of transportation and handling is relatively lower compared to steels. All of these advantages will decrease the cost of marine and coastal projects effectively [25]. After that, various different researches were carried out in this area. Some researchers suggested the sea-sand concrete filled FRP tubular column was a suitable application addressing durability and constructability. The ultimate compressive strength of concrete was proved to be increased due to the effective FRP confinements, but an obvious degradation in hoop strength was observed for GFRP and BFRP when exposed to artificial seawater environment [26]. Besides, the theoretical model was proposed by Li et al. [27] to analyze the behavior of FRP tube confined columns under axial compression. Other experimental studies focused on the FRP bars reinforced sea-sand based components, but they are mainly about beams. The sea-sand concrete beams reinforced with basalt FRP (BFRP) bars was demonstrated to have good flexural and shear behaviors [28]. Moreover, the experiments conducted by Dong et al. [29] showed that the failure mode of BFRP beams changed from concrete crushing to shear failure after immersion in 50 °C seawater for longer than 6 months, the contribution of BFRP stirrups to shear resistance capacity decreased.

For the application of SSC in marine and coastal areas, the SSC structures should own adequate stiffness to resist strong wind and earthquake, particularly for the high-rise building. As the shear wall structure is always the optimal option as the lateral force resisting member for its excellent load carrying capacity and seismic behavior, it is of great significance to investigate the structural behavior of SSC shear wall. Considering the corrosion problems, the FRP bars should be used to replace steel bars, including the longitudinal bars, transverse reinforcement, and stirrups. Unlike the steel reinforcements, FRP bars have no plastic deformation before reaching their ultimate tensile strength, and their stress-strain relationships are linearly elastic. So their application in concrete can be expected to control the residual deformation of the structure after the earthquake. Most of the current researches focus on the conventional concrete shear wall reinforced with FRP bars, but few on the SSC shear wall. The experimental study conducted by Chen [30] provided an analysis on five conventional concrete shear walls under quasi-static cyclic loading, of which the specimens were partly or totally reinforced by CFRP bars in the longitudinal direction. The results demonstrated that the ultimate bearing capacity of shear walls could be met through the reasonable

configuration of CFRP bars, and the CFRP could improve the pattern of the crack distribution as well as control the crack width. The test conducted by Mohamed et al. [25] presented four full-length conventional concrete shear walls with different high span ratios (three GFRP-reinforced and one steel reinforced). The results indicated that the level of energy dissipation of GFRP-reinforced shear wall was acceptable as compared with that of the steel reinforced one. Moreover, the results of numerical simulation on these GFRP-reinforced walls showed that the shear related damage could be primarily controlled due to the elastic behavior of GFRP bars [31]. Arafa et al. [32] conducted a test of six full-scale GFRP-reinforced concrete squat walls under quasi-static reversed cyclic loading, and the results also showed that the horizontal and vertical web GFRP bars could control the shear crack width. Overall, it can be generally summarized that the application of steel bars in structures has higher energy dissipation for its plastic deformation, while the FRP bars can be used without sizeable residual deformation and cracks in addition to the ultimate bearing capacity and reasonable energy dissipation level.

This study is experimental research on the structural behavior of SSC shear wall reinforced with GFRP bars. It aims to mainly evaluate the feasibility of using FRP bars in SSC structures. The seismic test is carried out on the SSC shear walls, and the specimen is designed by the requirements of GB50011-2011 [33]. The objective is to demonstrate that the SSC shear wall reinforced with GFRP bars can reach the deformability requirements as well as a reasonable bearing capacity.

2. Seismic tests of seawater sea-sand concrete shear wall

2.1. Experimental program

The ribbed GFRP bars were chosen in this study with the stirrups processed by GFRP material, as shown in the Fig. 1. The GFRP is of high strength and high chemical resistance. Besides, its cost is relatively lower as compared to other types of FRP materials, such as carbon FRP (CFRP), basalt FRP (BFRP) and aramid FRP (AFRP), which makes it more common in construction engineering [34]. The seismic tests specimens contained three concrete shear walls, including NAC reinforced with steel bars (SNW), NAC reinforced with GFRP bars (GNW) and SSC reinforced with GFRP bars (GSW). The specimens were designed with enough reinforcement to ensure the domination of flexural behavior and avoid the failures of shear and sliding.

2.1.1. Design and details of shear wall specimens

The aspect ratio of all specimens was kept at the same value of 3.7, which classified as high-rise walls. They were 2400 mm in height (h_w), 800 mm in length (l_w) and 100 mm in thick (b_w). Besides, there were embedded columns on both sides. As shown in Fig. 2, the specimens were set with the top loading beam and the bottom basis. The top loading beam was used to apply the vertical and transverse force, and the bottom basis was used for fixing. The three shear walls have the same concrete dimensions and reinforcement ratio, as presented in Fig. 3. The SSC was made by totally replacing the freshwater and river sand with seawater and unwashed sea-sand. The used GFRP and steel bars were of the same diameter to keep the same reinforcement ratio. Research [17] showed that axial-reinforcement stiffness (EA) governs the flexural behavior of FRP reinforced concrete members, but

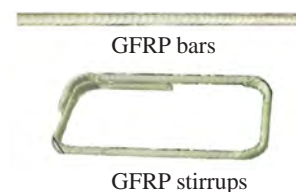


Fig. 1. GFRP bars and stirrups.

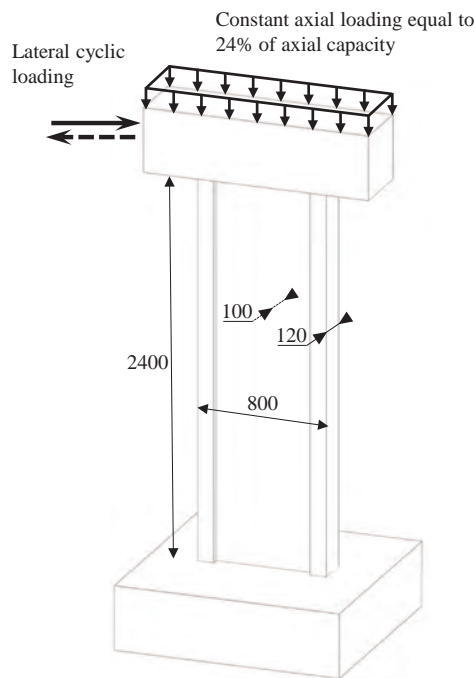


Fig. 2. Dimensions of shear walls (mm).

compared to that of steel bars reinforced concrete, the GFRP bars reinforced concrete was always over-reinforced since the elastic modulus of GFRP bars were lower. The feasibility of completely replacing the steel bars with the GFRP bars of the same diameter and reinforcement ratio in shear walls was studied.

2.1.2. Material properties

Table 1 shows the mix proportion of the concrete. Ordinary Portland cement was used in this study. Table 2 shows the detailed properties of the used fine aggregate, and the sea-sand was derived from Fujian Province, China. It can be found that the content of shells and the chemical substances in sea-sand is relatively higher. As shown in Fig. 4, the grading curve of the sea-sand does not conform to standard grading [35]. Table 3 presents the chemicals to be added in freshwater for producing simulated seawater, which is presented by ASTM D1141-98 [36]. Also, Table 4 shows the properties of natural coarse aggregate. 150 mm cubes and 150 mm × 150 mm × 300 mm prisms were cast and cured under the same condition to obtain the cubic compressive strength and the full compressive stress-strain curve. Fig. 5 shows the comparison of the full compressive stress-strain curve, the peak compressive strength of SSC is a bit larger than that of NAC, but generally, they present a similar trend. For the reinforcing materials, 6-mm and 10-mm steel bars were used in SNW, and the GFRP bars were of the same diameter size. The 10-mm bars were used as longitudinal bars during the 6-mm ones as the transverse reinforcements and stirrups. The mechanical properties of the used reinforced bars were determined according to GB/T228-2010 [37] (for metal materials) and JG/T406-2013[38] (for FRP materials), and the results are presented in Tables 5 and 6, respectively, while Fig. 6 shows the comparison of tensile stress-strain curves.

2.1.3. Test apparatus and procedure

The test apparatus is shown in Fig. 7. Reaction frame was used to transfer the applied axial and lateral loads. The out-of-plane displacement of specimens was prevented and did not influence in-plane displacement. During the test, the axial load of approximately $0.24A_w f_c$ maintained constant, and it was applied evenly through the top beam to the specimen by a hydraulic jack. Meanwhile, a cyclic lateral displacement was applied on specimens with a 2000 kN MTS actuator. The

quasi-static reversed loading procedure is shown in Fig. 8, and the number of cycles at each lateral drift is presented in Table 7. The push direction of the actuator was defined as positive (+) while the pull direction as negative (-), and the test started at the positive load.

On the specimens, a series of LVDTs and strain gauges were used to obtain the response of the shear walls, as presented in Fig. 9. The lateral displacements at the top beam (D1) and the wall height (D2) were measured. There were two LVDTs used for recording the displacement at different height of the wall (D3 and D4). Moreover, the horizontal sliding between the base and the rigid floor was also measured (D5), although it was unlikely to occur. Besides, the development of cracks was carefully marked and recorded during the tests.

2.2. Test results

2.2.1. Crack propagation and failure patterns

During the test, neither the anchorage failure nor the sliding displacement was observed. The crack propagation of the specimens after failure is shown in Fig. 10. It can be seen that all the cracks are distributed within the range from the base of the wall to the two-third height of wall. The cracks on and between the embedded columns are mainly horizontal and diagonal cracks, respectively, and part of the horizontal cracks extends from both ends of the wall. The spacing of horizontal cracks for SNW is narrower than that of GNW and GSW. The angle of the diagonal cracks increases from the bottom to the top from 20° to 50° relative to the horizontal.

The failure process of specimens and the corresponding displacement are shown in Table 8. Besides, Figs. 11 and 12 present the failure process of the embedded columns bottom during the test. For SNW, the procedure was described as follows. When the applied displacement was less than 4.8 mm (lateral drift < 1/500), no cracks were observed. The first horizontal crack appeared until the lateral displacement was 4.8 mm. Then more horizontal cracks appeared and extended gradually, the first flexure-shear crack happened at the displacement of 12 mm (lateral drift = 1/200). As the applied displacement reached 36.9 mm (lateral drift = 1/65), no new cracks were observed, the extension of the existing cracks became slow. Subsequently, the vertical cracks showed up at the bottom of the embedded columns, and the concrete began to spalling from the surface. When the applied displacement increased to 48 mm (lateral drift = 1/50), the longitudinal bar in the embedded columns was exposed, and the specimen reached its peak load capacity. Finally, the concrete was crushed, and the longitudinal bar was bent considering the specimen failed.

For GNW and GSW, their failure process was similar. It seems that the use of SSC does not influence the crack propagation. The first horizontal crack of SSC appeared later than that of SNW ($\Delta = 6$ mm, lateral drift = 1/400) due to their different bond behaviors. The first flexure-shear crack also happened at the displacement of 12 mm (lateral drift = 1/200). Then the vertical cracks at the bottoms appeared along with the spalling of the concrete, with the displacement increased to 30 mm (lateral drift = 1/80), which happened earlier than the steel reinforced walls. When the displacement was further increased to 48 mm (lateral drift = 1/50), new cracks showed up and the concrete surface of the embedded column was spalling, the specimens reached its peak load capacity. About GNW, the concrete was crushed soon, the load capacity suddenly decreased and the longitudinal GFRP bars as well as stirrups failed by shearing. The GSW was tested to failure at the lateral displacement of 60 mm (lateral drift = 1/40) with the similar failure process.

2.2.2. Strain analysis

The measured strains of longitudinal, transverse bars and stirrups are shown in Figs. 13–15. It can be seen from Fig. 13 that the longitudinal strain growth rates of GNW and GSW are similar to that of SNW, as the applied displacement is the same. The steel bars reached the yield strain at 24 mm with the strain gauge failed afterward. On the

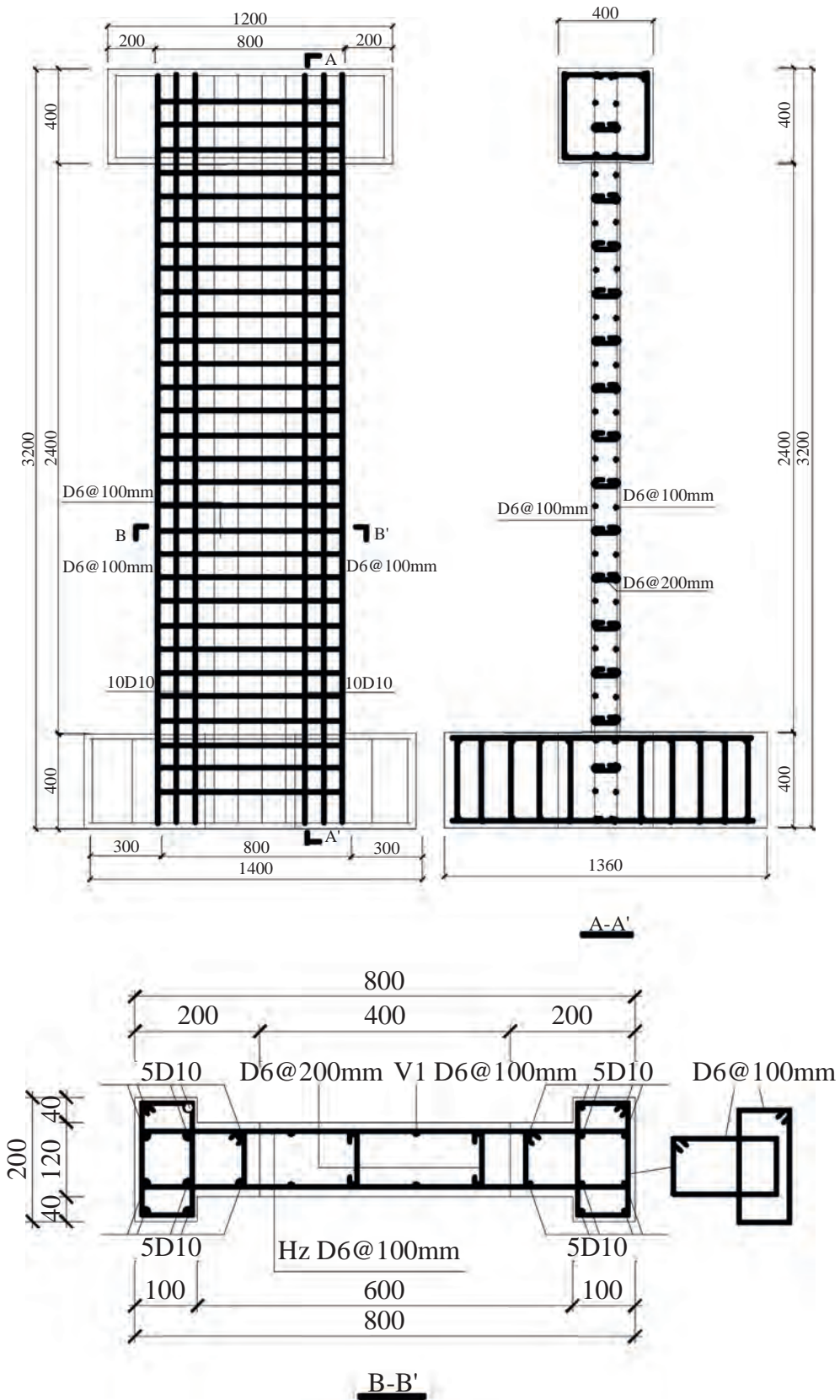


Fig. 3. Details of reinforcements (mm).

Table 1
Mix proportion of concrete.

Type	Water cement ratio	Water (kg/m ³)		Cement (kg/m ³)	Fine aggregate (kg/m ³)		Coarse aggregate (kg/m ³)	Water reducer (kg/m ³)
		tap water	seawater		river sand	sea-sand		
NAC	0.47	150	0	319	829	0	1099	2.87
SSC	0.47	0	150	319	0	829	1099	2.87

Table 2
Material properties of fine aggregate.

Type	Apparent density (kg/m ³)	Fineness modulus	Content of Cl ⁻ (%)	Content of shells (%)	Content of SO ₃ (%)
River sand	2610	2.1	0.001	1.10	0.109
Sea-sand	2660	2.7	0.057	2.31	0.123

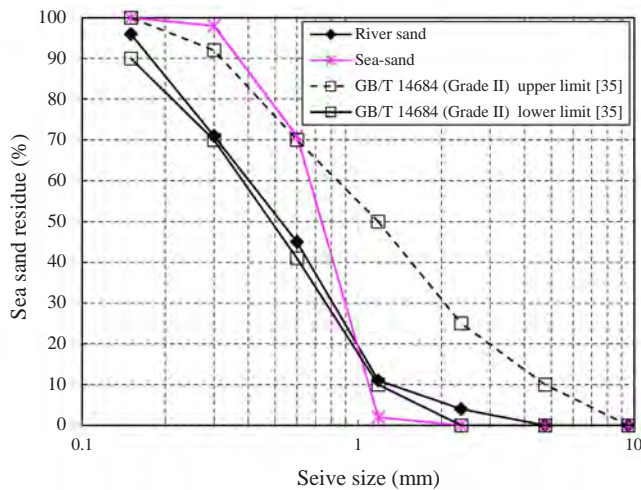


Fig. 4. Grading curves of the sands [35].

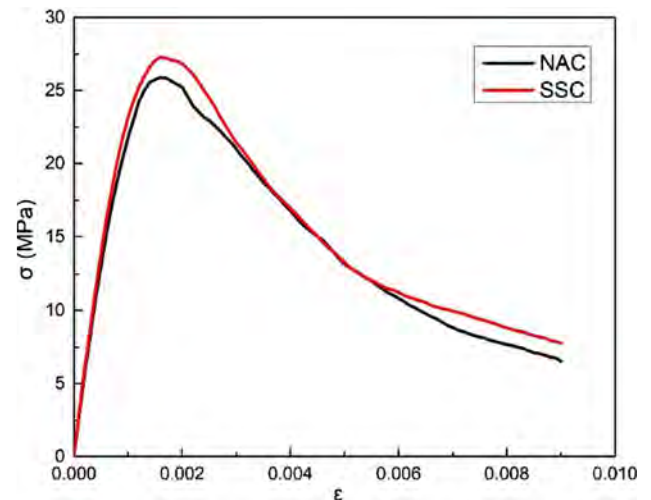


Fig. 5. Stress-strain curve of NAC and SSC.

Table 3
Chemical composition of simulated seawater.

Compound	NaCl	MgCl ₂	Na ₂ SO ₄	CaCl ₂	KCl	NaHCO ₃	KBr
Concentration (g/L)	24.53	5.20	4.09	1.16	0.695	0.201	0.101

*The content of chemical substance below 0.1 g/L is ignored.

Table 4
Material properties of natural coarse aggregate.

Apparent density (kg/m ³)	Bulk density (kg/m ³)	Content of clay (%)	Water absorption (%)	Crush index
2660	1360	0.8	1.0	5.1

contrast, the strain of GFRP bars continued to increase with a sudden change occurred for GNW and GSW after the respective displacement of 36.9 mm and 48 mm, which is consistent with the failure process of the tested specimens. From Fig. 14, it can be noticed that the transverse bar strains of GNW and GSW have a similar tendency and they are significantly higher than that of SNW after cracking. This is due to the lower modulus of GFRP bars than that of steel bars ($E_f \approx 1/4E_s$). The stress of transverse steel bars became constant after the displacement of about 20 mm, this may be contributed to the yielding of the specimens, while the strain of GFRP bars continued increasing until the specimen failed. The stirrups were used as confinements to improve the mechanical behavior of concrete. It can be found in Fig. 15 that the slope of the stirrup strain-displacement curve increased obviously when the

concrete was fractured under compression. The stirrup strains of GNW and GSW were also larger than that of SNW for the lower elastic modulus of GFRP bars. The stirrups in GNW behaved the same as that in GSW in the push direction, but the behaviors were not the same in the pull direction. It may be related to the character of the GFRP stirrups, which were processed by the GFRP rod in this test. According to the research conducted by Dong et al. [21], the rod stirrups are characterized by at least one side overlap, where premature bond slip failure is likely to occur, resulting in low confinement efficiency. It seems that the GFRP stirrup in SNW lost its effect bond with concrete in push direction, leading to the difference behavior of SNW. However, this still needs to be studied further, such as the behavior of different GFRP stirrup forms. Besides, a sudden drop of stirrup strain for GNW happened at 36.9 mm, it may be because that there were some weak points existed in the GFRP stirrups, and this may be a reason for the earlier failure of GNW compared to GSW.

2.2.3. Hysteresis curves

The hysteresis curves of the shear wall specimens are obtained to evaluate the seismic performance of shear wall [39], as shown in Fig. 16. Before cracking, the curves present as a thin and slender ring shape and their enclosed areas are small, which means the specimens are in the elastic stage. After cracking, they begin to present nonlinear behavior. With the increase of applied displacement, the area surrounded by the hysteresis loop becomes larger. Obvious residual deformation can be observed when the lateral load back to zero. The SNW and GFRP bars reinforced specimens behave differently in the nonlinear stage. The hysteresis loop of SNW acts as a spindle shape, while the

Table 5
Mechanical properties of steel bars.

Type	Diameter (mm)	Test yield strength f_y (MPa)	Test ultimate strength f_u (MPa)	Elasticity modulus E_s (GPa)
HPB300	6	505.0	630.0	209
HRB400	10	543.3	669.1	213

Table 6
Mechanical properties of GFRP bars.

Type	Diameter (mm)	Tensile Strength f_f (MPa)	Elasticity modulus E_f (GPa)	Rib spacing (mm)	Rib height (mm)
B100-6	6	1191.3	50.3	6	2
B100-10	10	794.9	45.8	10	3

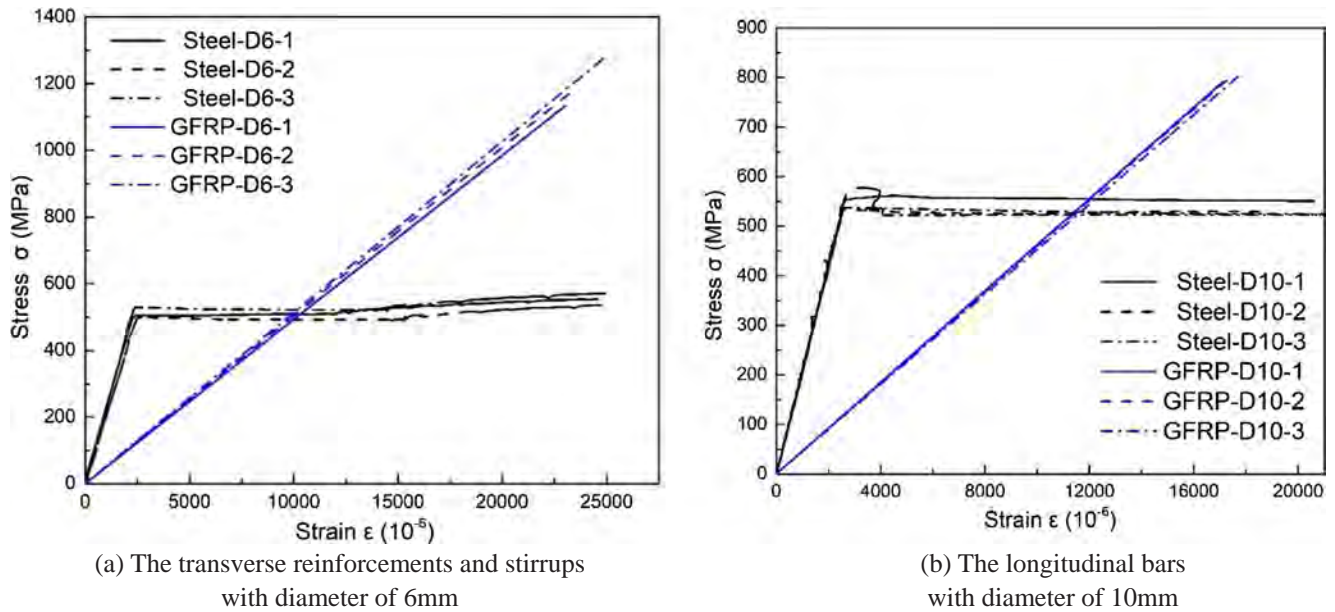


Fig. 6. Stress-strain curves of reinforcing bars.

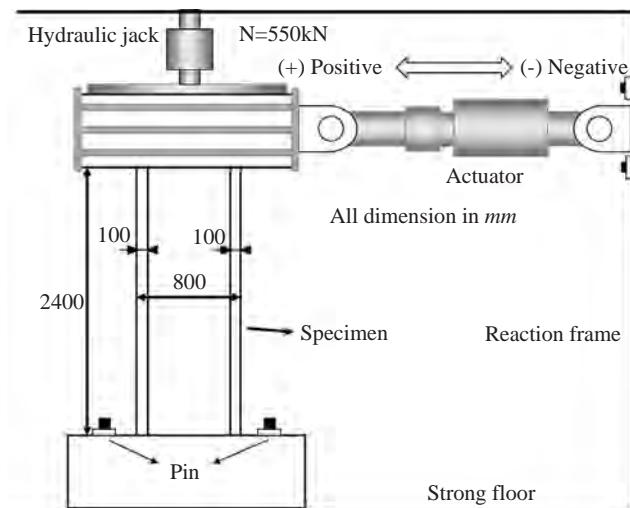


Fig. 7. Test apparatus of seismic test for shear wall.

GNW and GSW present as an S-shape. It shows that the replacement of steel bars with GFRP bars in the shear wall reduces its energy dissipation behavior. Besides, the influence of the SSC on the hysteresis curves is slight.

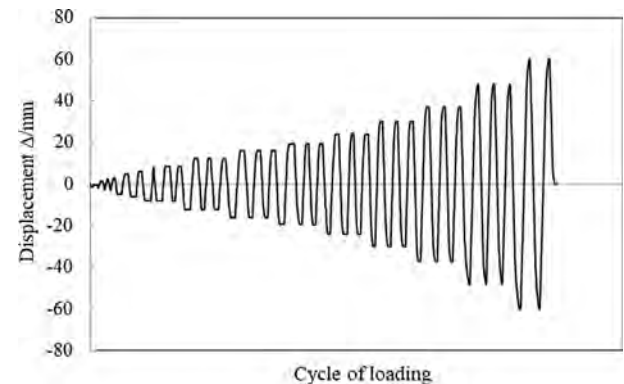


Fig. 8. Applied cyclic lateral displacement on shear walls.

2.2.4. Envelope curves

The envelope curve is obtained by connecting the peak point of the first cycle at each load step in hysteretic curve [40], as shown in Fig. 17. It can be seen that the shape of the curves for GNW and GSW are similar, which indicates that the influence of using SSC in the shear wall is not significant. At the elastic stage, the load and displacement have a linear relationship. After cracking, the curves show an obvious turning point, which shows the degeneration of stiffness. The load further increases with the applied displacement until the peak point is reached.

Table 7
Applied lateral displacement on shear walls.

Lateral drift	1/1000	1/800	1/500	1/400	1/300	1/200	1/150	1/125	1/100	1/80	1/65	1/50	1/40
Displacement (mm)	2.4	3	4.8	6	8	12	16	19.2	24	30	36.92	48	60
Number of cycles	1	1	1	1	3	3	3	3	3	3	3	3	3

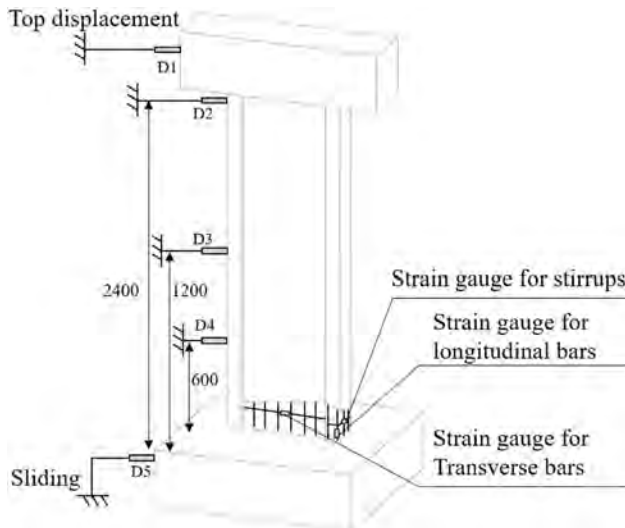


Fig. 9. Layout of measuring device on shear wall (mm).

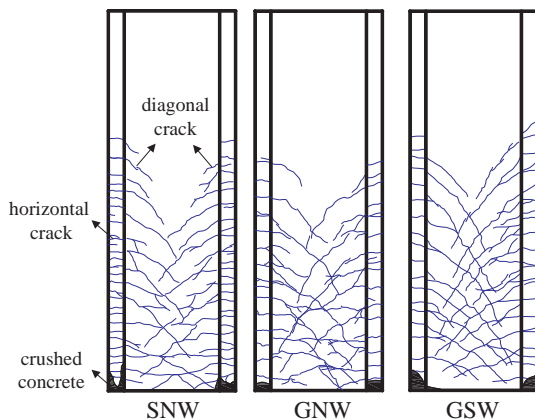


Fig. 10. Crack propagation of shear walls.

After that, the curve suddenly drops as the specimen is tested to failure. Compared with GNW and GSW, SNW has a larger envelope curve. Besides, the slope of SNW curves is larger than that of GNW and GSW at the beginning of loading, indicating that the initial stiffness of steel reinforced shear wall is greater than GFRP reinforced. When the peak load is reached, there is a certain yield stage in SNW as the load remained unchanged with the increase of top displacement. On the contrary, the GFRP reinforced specimens show a sudden drop curve, and this is due to the property of GFRP bars. By replacing the steel bars by the GFRP bars in the same dimensions, the specimen's peak load capacity decreases, but all the three specimens can reach the lateral drift of 1/50, which demonstrates that all the specimens can meet the deformation requirements.

2.2.5. Load capacity and the characteristic value

The characteristic points of yield, peak and ultimate loads are determined by the envelope curve. In particular, the yield point for GFRP specimens is obtained according to the energy equivalence method [41,42], as shown in Fig. 18. Assuming the original curves as a two-line

Table 8
Failure progression of shear walls.

Test phenomenon	Specimen	Δ^* (mm)	Lateral drift ^{**}
First crack	SNW	4.8	1/500
	GNW	6	1/400
	GSW	6	1/400
Flexure-shear crack (diagonal crack)	SNW	12	1/200
	GNW	12	1/200
	GSW	12	1/200
Vertical crack at bottom of embedded column	SNW	36.9	1/65
	GNW	30	1/80
	GSW	30	1/80
Cracks were fully developed	SNW	36.9	1/65
	GNW	48	1/50
	GSW	48	1/50
Concrete crushing	SNW	60	1/40
	GNW	48	1/50
	GSW	60	1/40

* Δ = Lateral top displacement (mm).

** Lateral drift = Δ/h_w .

model (OB-BP), and let them have the same energy dissipation, i.e., to make the areas of the two envelope curves the same. And the displacement of point B is taken as the yielding displacement, the corresponding point of the original curves is taken as the yielding point. The peak load P_m (kN) is the maximum bearing capacity of the specimen, and the corresponding displacement is the peak displacement Δ_m (mm). The ultimate point is determined as the point when the load drops to about 85% of the peak load. Specifically, if the load does not fall to 85% after failure, the peak point is taken as the ultimate point. The calculated load capacity and the characteristic value of displacement are shown in Table 9.

As for the yield point, the GFRP reinforced SSC shear wall is comparable to the conventional concrete specimen. Moreover, compared with SNW, their yield loads are lower while the corresponding displacements are larger. For the peak point, the peak loads of GNW and GSW are smaller than that of SNW, which are about 88% and 84% of the SNW in a positive direction while 87% and 91% of the SNW in the negative direction, respectively. However, the corresponding peak displacements of GFRP reinforced specimens are relatively higher. The envelope curve of SNW declines slowly to the ultimate point while the GNW and GSW suddenly fail after the peak point. The lower bearing capacity of GFRP reinforced specimens is mainly because the ultimate stage of the specimens is characterized by concrete crushing, when the concrete reaches the ultimate compressive strain, the corresponding tensile stress of GFRP does not reach its tensile strength, and it is also less than that of steels.

Ductility coefficient is calculated using the Eq. (1).

$$\mu = \Delta_u / \Delta_y \tag{1}$$

where the Δ_u (mm) is the ultimate displacement, and Δ_y (mm) is the yield displacement.

The ductility coefficient of SNW is 4.91 whereas the GNW and GSW specimen coefficient is 2.47 and 2.68, respectively. It shows that the SSC has a negligible influence on the ductility behavior of shear walls. The GFRP reinforced shear walls have poorer ductility behavior which presents a brittle failure mode.

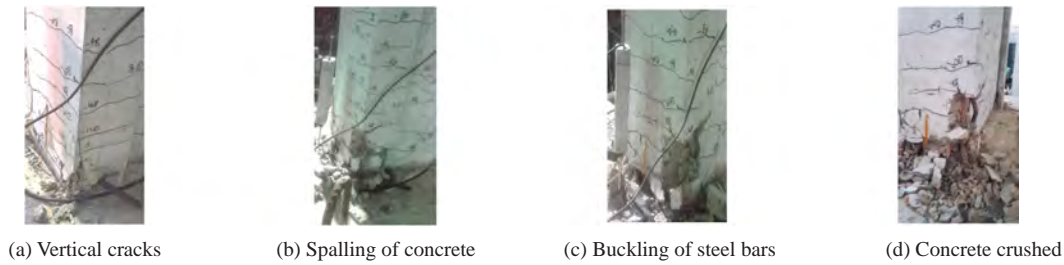


Fig. 11. Failure process of SNW.

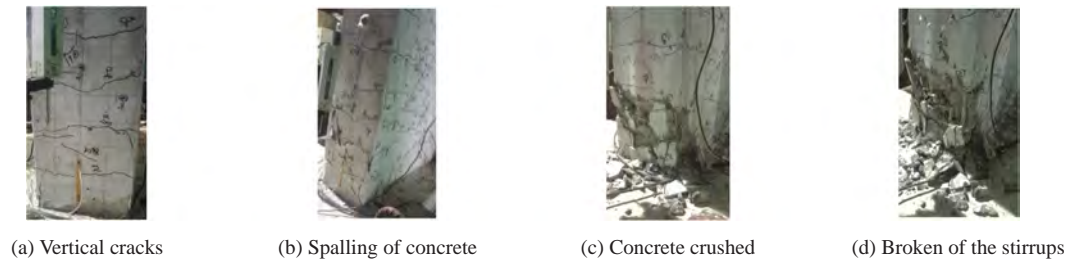


Fig. 12. Failure process of GNW and GSW.

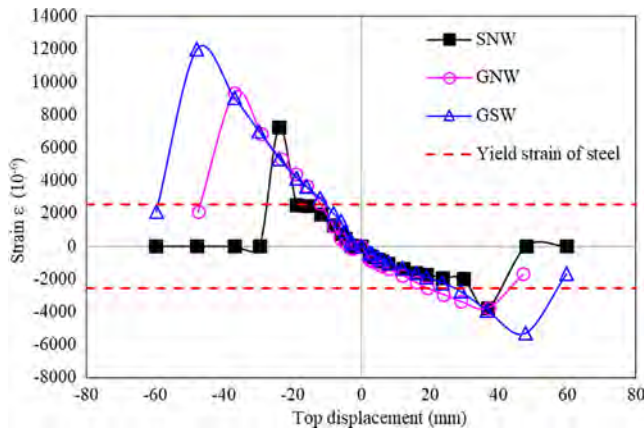


Fig. 13. Development of strain for longitudinal bars in embedded columns.

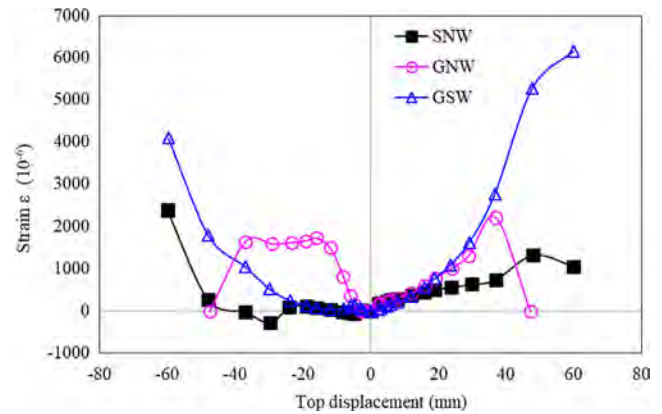


Fig. 15. Development of strain for stirrups.

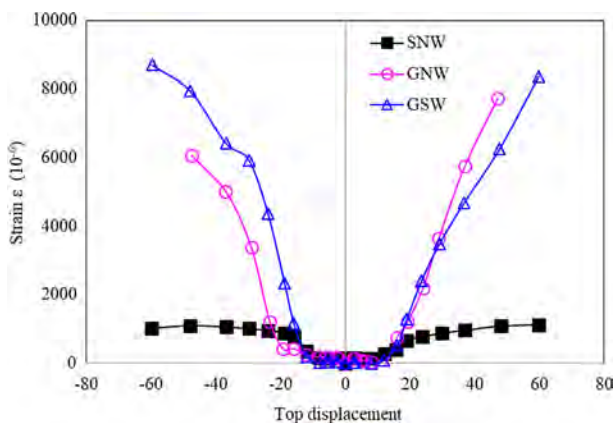


Fig. 14. Development of strain for transverse bars.

2.2.6. Stiffness degradation

Secant stiffness is used to represent the stiffness of specimens and is calculated by Eq. (2) [43]. The results are shown in Fig. 19.

$$K_i = \frac{|+F_i| + |-F_i|}{|+X_i| + |-X_i|} \quad (2)$$

where the $+F_i$ and $-F_i$ are the positive and negative peak load values at the cycle i , while $+X_i$ and $-X_i$ are the corresponding displacement.

It can be seen that the initial stiffness of SNW is larger than that of GNW and GSW, this is mainly because of the lower elastic modulus of GFRP bars. The curves of the GNW and GSW are nearly identical, which indicates SSC has little influence on the stiffness. All the specimens have the same degradation trend. The degradation of stiffness is fast at the beginning, but it slows down as the specimens enter the yield phase. Especially, after the vertical cracks appear at the bottoms, the stiffness degradation tends to be gentle. The stiffness difference between the specimens become minimal when the specimens are nearly tested to failure.

2.2.7. Energy dissipation

The area of the first hysteresis loop at each loading stage is calculated to represent the energy dissipation, as shown in Fig. 20. At the initial stage, all the three specimens have small values and slow growth of energy dissipation, their energy dissipation curves almost coincide with each other. After that, the energy dissipation of SNW increases rapidly and presents a linear growth, while that of GNW and GSW increase at the same rate as the initial stage. Besides, the energy dissipation curve of the GSW is also comparative to that of the GNW, and they are visibly lower than that of the SNW. It seems that the substitution of SSC does not decrease the energy dissipation capacity of the

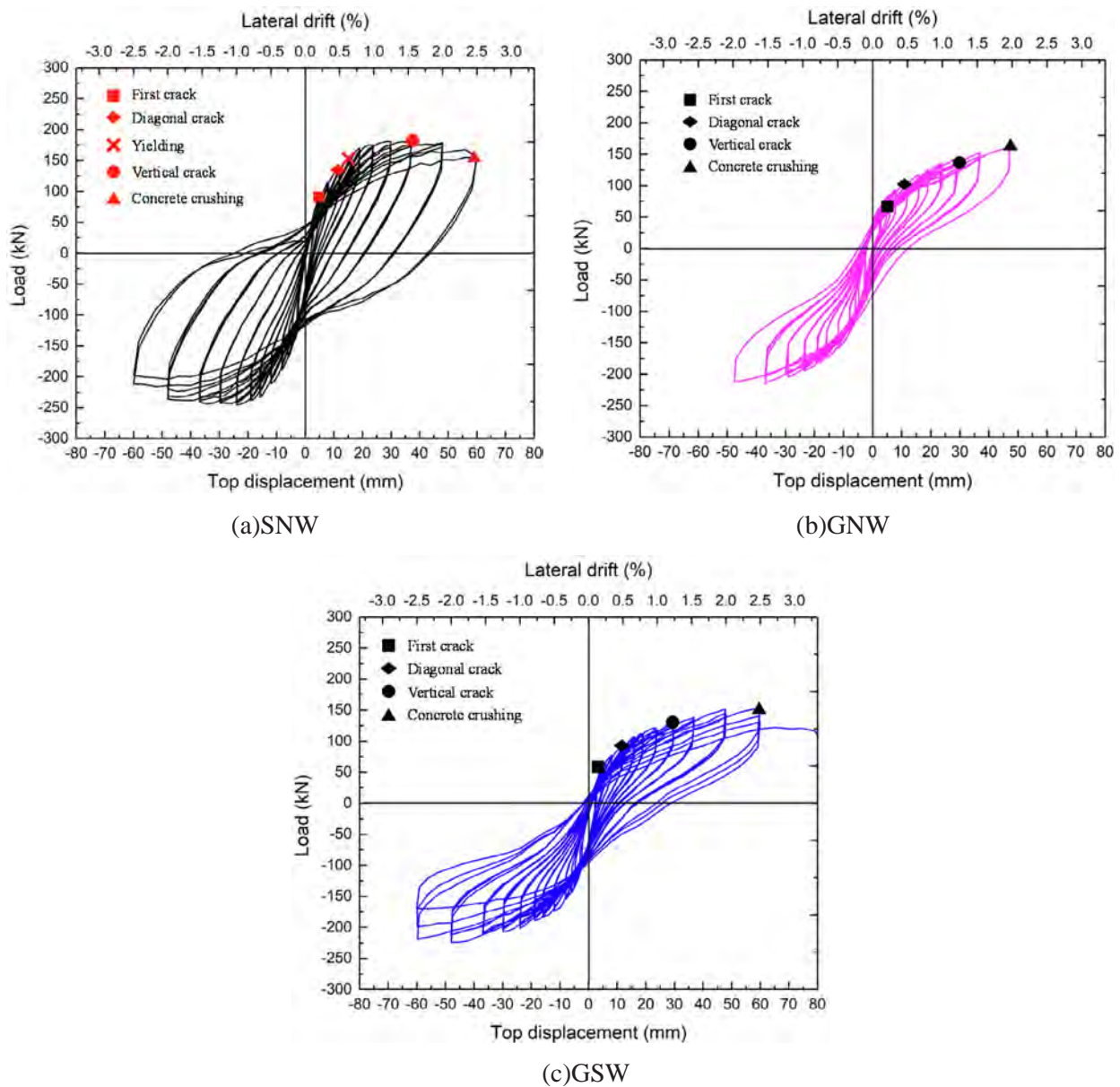


Fig. 16. Hysteresis curves.

shear wall.

Also, the equivalent viscous damping coefficient h_e is calculated by Eq. (3) [43] with the schematic graph shown in Fig. 21.

$$h_e = \frac{A_1}{2\pi(A_2 + A_3)} \quad (3)$$

where A_1 is the area surrounded by the hysteresis ring BADC, A_2 is the area of the triangle OBE, A_3 is the area of the triangle ODF.

As shown in Fig. 21, the h_e of the SNW is higher than that of the GNW and GSW on the whole, demonstrating the SNW has fuller hysteresis curve and thus the higher energy dissipation capacity. Moreover, the h_e of the GSW specimens can also reach the level of GNW.

2.2.8. Deformation pattern and lateral residual deformation

The deformation shapes of the specimens are analyzed with the data obtained from the LVDTs. As presented in Fig. 22, the lateral displacement of specimens is set as the abscissa during the height of the wall as the ordinate. Deformation at the lateral drift of 1/100 and 1/50 are compared, and it presents that the lateral displacement curves of the three specimens are slightly differences, but all of them show typical

bending type deformation. It confirms that both the steel and GFRP reinforced shear wall is dominated by flexure effects in this test.

The lateral residual deformation is obtained from the measured hysteresis curve by taking the displacement at the end of each loading step, namely the corresponding displacement when the load dropped to zero. The comparison is shown in Fig. 23, and it can be seen that, when the applied displacement is less than 19 mm, the lateral residual deformations of the specimens are almost the same, and their value is small. As the steel bars enter the yield phase, the residual deformation of the SNW increases significantly, while the growth of the GNW and GSW are far less than that of the SNW. When the lateral drift reaches 1/50, the residual deformation of SNW is 23.6 mm, while the GNW and GSW were 8.4 mm and 8.9 mm respectively. The deformation of GSW can be effectively recovered after unloading, and it presents a linear relationship as the load applied, which is similar to that of the GNW.

2.3. Bearing capacity analysis of seawater sea-sand concrete shear wall

The bearing capacity of SSC shear wall reinforced with GFRP bars is

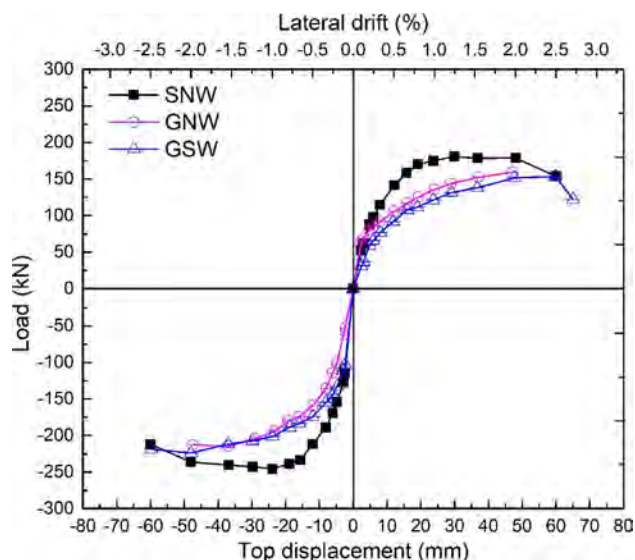


Fig. 17. Envelope curves.

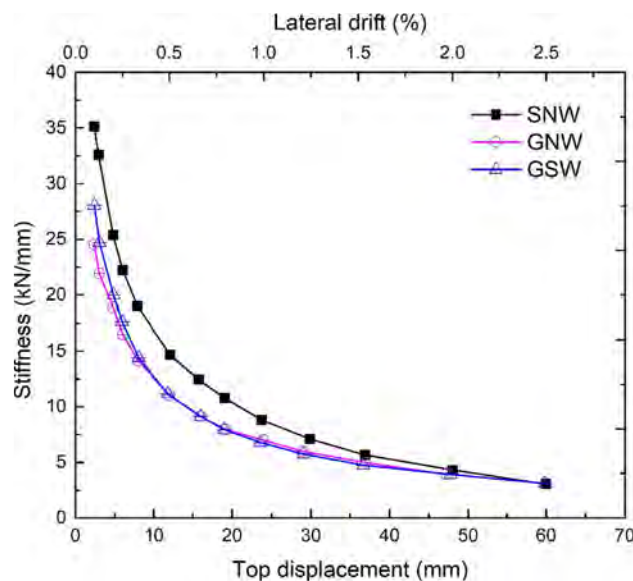


Fig. 19. Stiffness degradation curves.

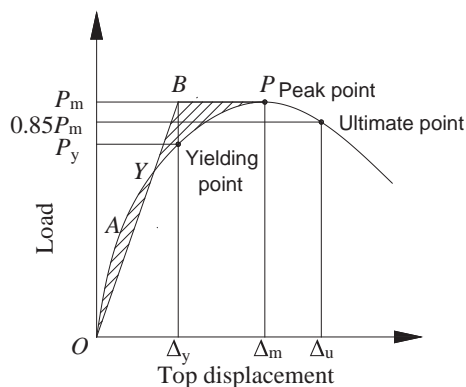


Fig. 18. Yielding point [41,42].

proved to be comparable to that of the conventional concrete shear wall. Moreover, the existing design method is used to verify the applicability on the SSC shear wall.

2.3.1. Flexural capacity

The flexural capacity of the shear wall reinforced with GFRP is verified according to the code ACI 440.1R-15 [22] and GB 50608-2010 [23]. Generally, the failure mode can be determined by comparing the FRP reinforcement ratio ρ_f and balanced ratio ρ_{fb} . In this test, the ρ_f is larger than ρ_{fb} , so the failure of the specimen is initiated by the crush of concrete. As presented in ACI 440.1R-15, the distribution of stress in the concrete is approximated as a rectangular stress block, and the strain of FRP can be calculated by the plane cross-section assumption. Besides, the effect of FRP bars in compression zone is not considered

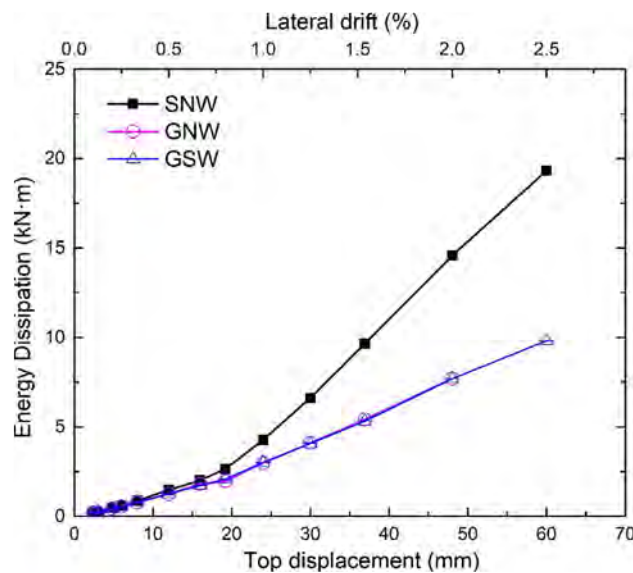


Fig. 20. Energy dissipation.

since the elastic modulus of GFRP bars is of the same magnitude as that of concrete. Based on the equilibrium of forces and ignore the effects of the web reinforcements, the following Eqs. (4) and (5) are derived.

Table 9

Characteristic load values of specimens.

Specimens	Loading direction	Yielding point		Peak point		Ultimate point		μ	Mean value of μ
		P_y (kN)	Δ_y (mm)	P_m (kN)	Δ_m (mm)	P_u (kN)	Δ_u (mm)		
SNW	Push(+)	152.0	14.6	180.6	29.9	157.0	58.5	4.00	4.91
	Pull(-)	-201.9	-10.3	-245.6	-24.0	-208.8	-60.0	5.82	
GNW	Push(+)	129.0	20.9	159.3	47.2	159.3	47.2	2.26	2.47
	Pull(-)	-177.8	-17.8	-214.5	-37.0	-182.3	-47.5	2.67	
GSW	Push(+)	125.0	25.7	153.6	59.8	130.6	64.0	2.49	2.68
	Pull(-)	-185.0	-16.7	-223.7	-48.0	-223.7	-48.0	2.87	

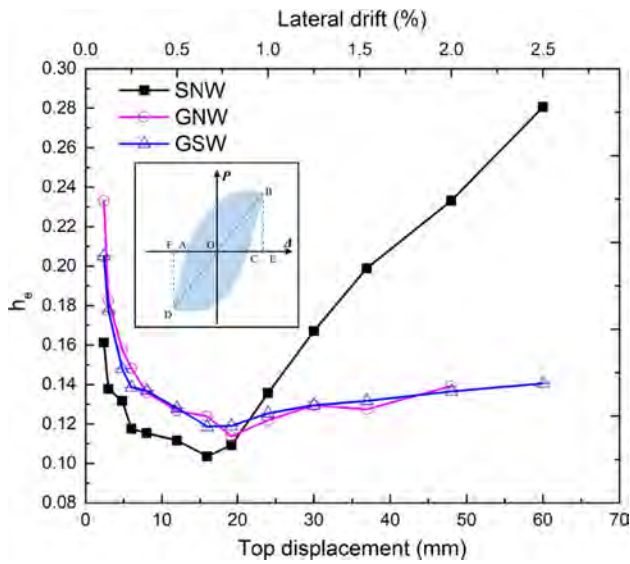


Fig. 21. Equivalent viscous damping coefficients.

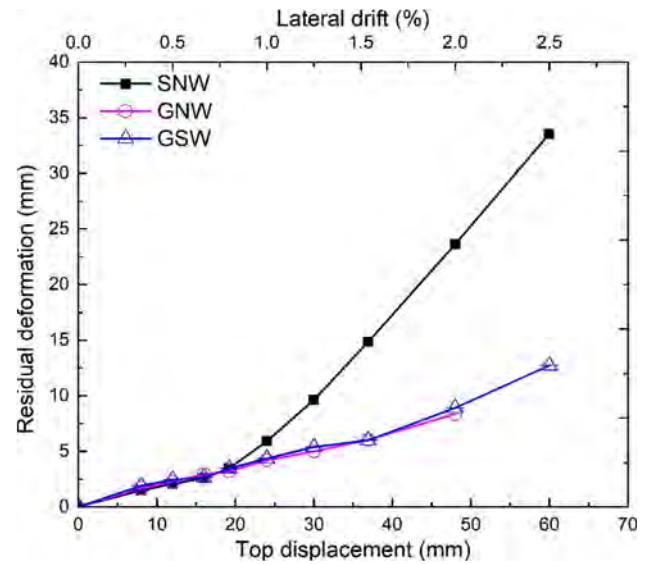


Fig. 23. Lateral residual deformation.

$$\sum N_i = 0 \begin{cases} N = N_c - A_f f_f \\ f_f = E_f \varepsilon_{cu} \frac{\beta_1 h_0 - x}{x} \\ N_c = \alpha_1 f_c b_w x + \alpha_1 f_c h'_f (b'_f - b_w) \end{cases} \quad (4)$$

$$\sum M_i = 0 \begin{cases} M_N + M_V = M_c \\ M_N = N \left(h_0 - \frac{h_w}{2} \right) \\ M_V = P \cdot H \\ M_c = \alpha_1 f_c b_w x \left(h_0 - \frac{x}{2} \right) + \alpha_1 f_c h'_f (b'_f - b_w) \left(h_0 - \frac{h'_f}{2} \right) \end{cases} \quad (5)$$

Where N is the applied axial pressure which is 550 kN, A_f is the area of the tensile GFRP bars, ε_{cu} is the ultimate strain of concrete which equals 0.003, f_c is the axial compressive strength of the concrete which is 26.20 MPa and 27.61 MPa for NAC and SSC respectively, h_{w0} is the distance from extreme compression fiber to centroid of tension reinforcement which equals 750 mm, b_w is the section width equals 120 mm, b'_f is flange width of compression zone equals 200 mm, h'_f is flange height of compression zone equals 100 mm, H is the height of the wall and P is the calculated lateral force.

The calculated P_1 is shown in Table 10. Also, considering the effects of the web reinforcements, the results P_2 can be obtained by updating

Table 10

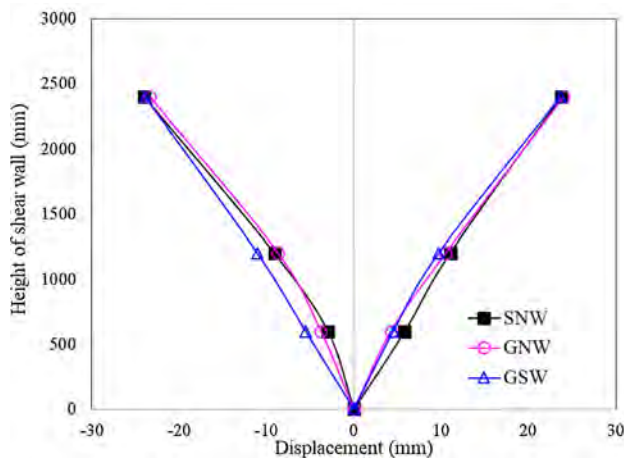
Comparison of the calculated values for flexural capacity.

Specimens	P_0 (kN)	P_1 (kN)	$\frac{P_0}{P_1}$	P_2 (kN)	$\frac{P_0}{P_2}$	P_3 (kN)	$\frac{P_0}{P_3}$
GNW	186.9	122.6	1.53	136.2	1.37	160.0	1.17
GSW	188.7	127.2	1.47	142.0	1.32	164.52	1.14

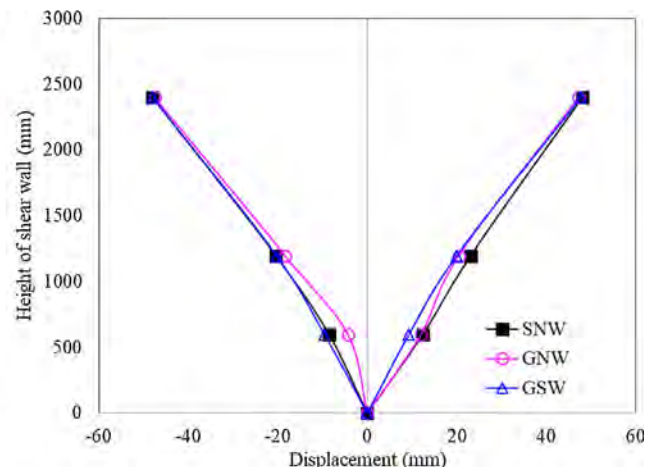
* P_0 is the test results, taking the average value of positive and negative bearing capacity. P_1 is calculated by ACI 440.1R-15 regardless of the effects of the web reinforcements while P_2 is the results after considering it. P_3 is calculated by GB 50608-2010 regardless of the effects of the web reinforcements.

the equations. The strain of all tensile bars is also determined by the assumption of the plane cross-section. It can be found that both the results are significantly larger than the test values, and the considering of web reinforcements reduces the difference by about 15%. It seems that the plane cross-section assumption may be not appropriate, as the aspect ratio of the shear wall is 3.

As for the GB 50608-2010, the actual stress of GFRP bars is determined according to the reinforcement ratio ρ_f with Eq. (6). And then the results P_3 are calculated by the equilibrium equation. This method also ignores the contribution of web reinforcements, but the results are much close to the experimental data. It can be concluded that all the



(a) Lateral drift at 1/100



(b) Lateral drift at 1/50

Fig. 22. Deformation patterns.

Table 11
Comparison of the calculated values for shear capacity.

Specimen	V_0 (kN)	ACI V_1 (kN)			GB V_2 (kN)			$\frac{V_0}{V_1}$	
		0.004	0.007	0.004	0.007	0.004	0.007	0.004	0.007
GNW	186.9	118.8	187.5	1.57	0.997	121.6	190.2	1.54	0.983
GSW	188.7	119.6	188.2	1.58	1.003	123.2	191.8	1.53	0.984

* V_0 is the test results, taking the average value of positive and negative bearing capacity. V_1 is calculated by ACI 440.1R-15 while V_2 is calculated by GB 50608-2010.

Table 12
Calculated value of proposed formula for shear capacity.

Specimen	Loading direction	Test results V_0 (kN)	V_0 (kN)	V_1 (kN)	$\frac{V_0}{V_1}$
GNW	Push (+)	146.2	177.1	160.1	1.11
	Pull (-)	-207.9			
GSW	Push (+)	134.5	163.2	161.7	1.01
	Pull (-)	-191.9			

existing theoretical calculation methods are conservative for calculating the flexural capacity of the SSC shear wall reinforced with GFRP bars.

$$f_f = \begin{cases} f_{fu} [1 - 0.211(\frac{\rho_f}{\rho_{fb}} - 1)^{0.2}] & (\rho_{fb} < \rho_f < 1.5\rho_{fb}) \\ f_{fu} (\frac{\rho_f}{\rho_{fb}})^{-0.5} & (\rho_f \geq 1.5\rho_{fb}) \end{cases} \quad (6)$$

2.3.2. Shear capacity

Although no shear failure occurred for each specimen, the shear bearing capacity is analyzed using the existing theory. The shear capacity is composed of the contribution of concrete and FRP, which is shown in Eq. (7).

$$V = V_c + V_f \quad (7)$$

where $V_c = 0.4\sqrt{f_c}kbh_0$ in ACI 440.1R-15 while $V_c = 0.86f_t bkh_0$ in GB 50608-2010, $V_f = f_{fv}A_{fv}h_0/s$, f_{fv} is the tensile stress of FRP for shearing design, A_{fv} is the amount of FRP shear reinforcement within spacing s , s is the space between shear reinforcement, f_t is the tensile strength of concrete and it is considered equals to $1/10f_c$ as the GB 50010 recommended [44], k is the influence coefficient of longitudinal reinforcement against shear capacity and it is calculated followed the standard.

Also, in order to control the shear crack widths, the stress of shear reinforcement is limited, which is expressed as $f_{fv} = 0.004E_f \leq f_{fb}$, where f_{fb} is the strength of the bent portion of FRP bars. However, the measured strain of transverse bars reaches to 0.007. The calculated results are shown in Table 11, and both the strain value of 0.004 and 0.007 are considered. It shows that the calculated values are lower than the test results when the strain value of 0.004 is used. However, if determined using the test strain of 0.007, the calculated values are much close to the test results.

In this test, the measured transverse reinforcement strain is much larger than 0.004, which is recommended in the specification. Considering the brittle failure characteristic of shearing effects and a specific safety coefficient, it is appropriate to control the strain at 0.004 in the design. At the same time, in order to make the calculation more accurate, it is suggested to consider the contribution of axial pressure, the shear capacity of FRP reinforced concrete can be described as follows.

$$V = 0.86f_t bkh_0 + 0.07N + \frac{f_{fb}A_{fv}}{s}h_0 \quad (8)$$

Where N (kN) is the axial loading. The test load of specimens when the transverse reinforcement at the strain of 0.004 is compared with the calculated value of Eq. (8), and the results are shown in Table 12. It can

be found that the calculated value is in good agreement with the measured result, so it is reasonable and recommended to use Eq. (8) to determine the shear capacity of the SSC shear wall reinforced with GFRP bars.

3. Discussion

From the tests above, the replacement of the conventional concrete by SSC has a little influence on the behavior of the shear wall. The GNW and GSW have a similar failure process, and other structural behaviors, which indicates the good feasibility of GFRP bars reinforced SSC shear walls. However, it still should be noticed that the shell content of the sea-sand and the long-term behavior of the SSC could influence the structural behavior of the shear wall or other components. The shell content of sea-sand is 2.31%, and it was proved to have a negligible influence on the mechanical behavior of SSC when the shell content is 10% [6]. As the shell content of sea-sand varies from different areas, the structural behavior of SSC using higher shell content sea-sand should be investigated. Besides, some researchers found that the mechanical behavior of GFRP bars reinforced specimen would decrease in seawater environment [26,29]. The long-term structural behavior should be stressed in further research.

On the other hand, it can be found that the space of the crack on the embedded columns for SNW is more compact than the GFRP reinforced specimens. It seems that the average bond stress between steel bars and concrete is larger than the GFRP bars according to Eq. (9) [45].

$$l_0 = \frac{f_t A_c}{\tau_b \Sigma u} \quad (9)$$

where the f_t is the tensile strength of concrete, τ_b is the average bond stress along the disturbed zone, A_c is the effective concrete area in tension, while the Σu is the perimeters of reinforcing bars.

However, the bond behavior is also influenced by the other factors, such as the diameter; some researches showed that the bond strength was decreased as the diameter increased [46]. There should be more researches on it, especially for the bond behavior in the long term.

4. Conclusions

This study is to evaluate the feasibility of using GFRP bars in sea-sand based concrete structures. Seismic behavior of the SSC shear wall reinforced with GFRP bars are investigated, and the results are promising concerning the applications of the seawater sea-sand concrete.

- (1) The replacement of conventional concrete with seawater sea-sand concrete in shear walls has a little influence on the structural behavior in the short term (shell content of sea-sand is 2.31%). The GNW and GSW specimens have similar failure patterns and shape of hysteresis curves. Considering the scarcity of conventional raw materials for concrete, the SSC can be a satisfied alternative of conventional concrete in structures, but more researches on the long-term behavior should be conducted.
- (2) The GFRP bars can be used to replace the steel reinforcement in the SSC shear walls, which solve the corrosion problems efficiently. It shows adequate load capacity and deformation ability with the

same reinforcement ratio as the steels. Both the load capacity of GNW and GSW can reach to over 85% that of SNW specimen and their lateral drift can be up to 1/50.

- (3) The replacement of steel bars with the GFRP bars reduces the energy dissipation of the shear wall. Due to the materials properties, the GNW and GSW show a brittle failure mode. The ductility factor of GNW and GSW is 2.47–2.68, which is lower than the 4.91 of SNW.
- (4) The GFRP reinforced shear walls present a lower residual deformation. As the lateral drift reaches 1/50, the residual deformation of SNW specimen is 23.6 mm while the GNW and GSW are 8.4 mm and 8.9 mm respectively, the use of GFRP bars could be a way to control the residual deformation of structures.
- (5) The flexural and shear capacity of SSC shear wall reinforced with GFRP bars are verified using the codes ACI 440.1R-15 and GB 50608-2010. The calculated results of flexural capacity are conservative, and they can be more accurate considering the contribution of web reinforcements. As for the shear capacity, the contribution of the axial load should be taken into account.

Acknowledgements

The authors wish to acknowledge the financial support from the National Natural Science Foundation of PR China (Project No: 51325802, 51438007) and the research grants from the National Natural Science Foundation of China (NSFC) (joint research project between NSFC and PSF, No. 51661145023).

References

- [1] Beauchemin S, Fournier B, Duchesne J. Evaluation of the concrete prisms test method for assessing the potential alkali-aggregate reactivity of recycled concrete aggregates. *Cem Concr Res* 2018;104:25–36.
- [2] Chau CK, Hui WK, Ng WY, Powell G. Assessment of CO₂ emissions reduction in high-rise concrete office buildings using different material use options. *Resour Conserv Recycl* 2012;61(4):22–34.
- [3] Kleijer AL, Lasvaux S, Citherlet S, Viviani M. Product-specific life cycle Assessment of ready mix concrete: comparison between a recycled and an ordinary concrete. *Resour Conserv Recycl* 2017;122:210–8.
- [4] Ioannidou D, Meylan G, Sonnemann G, Habert G. Is gravel becoming scarce? Evaluating the local criticality of construction aggregates. *Resour Conserv Recycl* 2017;126:25–33.
- [5] Xiao JZ, Qiang CB, Nanni A, Zhang KJ. Use of sea-sand and seawater in concrete construction: current status and future opportunities. *Constr Build Mater* 2017;155:1101–11.
- [6] Yang EI, Kim MY, Park HG, Yi ST. Effect of partial replacement of sand with dry oyster shell on the long-term performance of concrete. *Constr Build Mater* 2010;24(5):758–65.
- [7] Ma ZM, Zhao TJ, Zhao YD. Effects of hydrostatic pressure on chloride ion penetration into concrete. *Mag Concr Res* 2016;68(17):877–86.
- [8] Farahani A, Taghaddos H, Shekarchi M. Prediction of long-term chloride diffusion in silica fume concrete in a marine environment. *Cem Concr Compos* 2015;59:10–7.
- [9] Velegrakis AF, Ballay A, Poulos SE, Radzevičius R, Bellec VK, Manso F. European marine aggregates resources: origins, usage, prospecting and dredging techniques. *J Coastal Res* 2010;SI 51(6):1–15.
- [10] Zhou JL, Ou ZW, Chen Q, Chen Y. The influence of admixtures on the corrosion protection afforded steel reinforcement in seawater-and-seasand concrete. *Adv Mater Res* 2011;250–253:81–9.
- [11] Wang Z, Zhao XL, Xian G, Wu G, Raman RKS, Al-Saadi S. Durability study on interlaminar shear behaviour of basalt-, glass- and carbon-fibre reinforced polymer (B/G/CFRP) bars in seawater sea sand concrete environment. *Constr Build Mater* 2017;156:985–1004.
- [12] Lu XZ, Teng JG, Ye LP, Jiang JJ. Bond-slip models for FRP sheets/plates bonded to concrete. *Eng Struct* 2005;27(6):920–37.
- [13] Xiao JZ, Huang YJ, Sun ZH. Seismic behavior of recycled aggregate concrete filled steel and glass fiber reinforced plastic tube columns. *Adv Struct Eng* 2014:693–707.
- [14] Barris C, Torres L, Vilanova I, Miàs C, Llorens M. Experimental study on crack width and crack spacing for Glass-FRP reinforced concrete beams. *Eng Struct* 2017;131:231–42.
- [15] Al-saadi AU, Thiru A, Weena L. Structural applications of fibre reinforced polymer (FRP) composite tubes: a review of columns members. *Compos Struct* 2018;204:513–24.
- [16] Qasrawi Y, Hefferman PJ, Fam A. Performance of concrete-filled FRP tubes under field close-in blast loading. *J Compos Constr* 2015;19:04014067.
- [17] El-Nemr A, Ahmed EA, El-Safty A, Benmokrane B. Evaluation of the flexural strength and serviceability of concrete beams reinforced with different types of GFRP bars. *Eng Struct* 2018;173:606–19.
- [18] Maranan GB, Manalo AC, Benmokrane B, Karunasena W, Mendis P. Behavior of concentrically loaded geopolymer-concrete circular columns reinforced longitudinally and transversely with GFRP bars. *Eng Struct* 2016;117:422–36.
- [19] Guo R, Pan Y, Cai L, Hino S. Study on design formula of shear capacity of RC beams reinforced by CFRP grid with PCM shotcrete method. *Eng Struct* 2018;166:427–40.
- [20] Xie T, Mohamed Ali MS, Visintin P, Oehlers DJ, Sheikh AH. Partial interaction model of flexural behavior of PVA fiber-reinforced concrete beams with GFRP bars. *J Compos Constr* 2018;22(5):04018043.
- [21] Dong HL, Wang DY, Wang ZY, Sun YL. Axial compressive behavior of square concrete columns reinforced with innovative closed-type winding GFRP stirrups. *Compos Struct* 2018;192:115–25.
- [22] ACI440.1R-15. Guide for the design and construction of structural concrete reinforced with fiber-reinforced polymer (FRP) bars. ACI Committee 2015;440.
- [23] GB 50608. Technical code for infrastructure application of FRP composites. Beijing: China planning press; 2010. (in Chinese).
- [24] Zha XX, Cang YQ, Wang XL, Zhong ST. Investigation of steel-FRP-sea sand concrete stubs under axial compressive loading. *Build Struct* 2010;40(supplement):351–4. (in Chinese).
- [25] Mohamed N, Farghaly AS, Benmokrane B, Neale KW. Experimental investigation of concrete shear walls reinforced with glass fiber-reinforced bars under lateral cyclic loading. *ASCE J Compos Construct* 2014;18(3):A4014001.
- [26] Li YL, Zhao XL, Singh Raman RK. Mechanical properties of seawater and sea sand concrete-filled FRP tubes in artificial seawater. *Constr Build Mater* 2018;191:977–93.
- [27] Li YL, Teng JG, Zhao XL, Raman RS. Theoretical model for seawater and sea sand concrete-filled circular FRP tubular stub columns under axial compression. *Eng Struct* 2018;160:71–84.
- [28] Li SW. Experiment studies on the shear performance of sea sand concrete beam with BFRP tendons. Guangdong University of Technology; 2014. (in Chinese).
- [29] Dong ZQ, Wu G, Zhao XL, Zhu H, Lian JL. Durability test on the flexural performance of seawater sea-sand concrete beams completely reinforced with FRP bars. *Constr Build Mater* 2018;192:671–82.
- [30] Chen JW. Experimental study on the seismic behavior of CFRP-reinforced concrete shear wall. Zhengzhou University; 2015. (in Chinese).
- [31] Mohamed N, Farghaly AS, Benmokrane B. Numerical simulation of mid-rise concrete shear walls reinforced with GFRP bars subjected to lateral displacement reversals. *Eng Struct* 2014;73:62–71.
- [32] Arafah A, Farghaly AS, Benmokrane B. Effect of web reinforcement on the seismic response of concrete squat walls reinforced with glass-FRP bars. *Eng Struct* 2018;174:712–23.
- [33] GB50011. Code for seismic design of buildings. Beijing: China Architecture & Building Press; 2010. (in Chinese).
- [34] Gribniak V, Rimkus A, Torres L, Hui D. An experimental study on cracking and deformations of tensile concrete elements reinforced with multiple GFRP bars. *Compos Struct* 2018;201:477–85.
- [35] GB/T 14684. Sand for construction. Beijing; 2011. (in Chinese).
- [36] D1141–1998. Standard practice for the preparation of substitute ocean water. US-ASTM; 2013.
- [37] GB/T 228. Metallic materials-tensile testing. Beijing; 2011. (in Chinese).
- [38] JG/T 406. Glass fiber reinforced plastics rebar for civil engineering. Beijing: China Architecture & Building Press; 2013. (in Chinese).
- [39] Ashour A, Galal K, Farnia N. Analytical and experimental study on upgrading the seismic performance of reinforced masonry columns using GFRP and CFRP wraps. *J Compos Constr* 2018;22(4).
- [40] Deng K, Pan P, Shen S, Wang H, Feng P. Experimental study of FRP-reinforced slotted RC shear walls under cyclic loading. *J Compos Constr* 2018;22(4):04018017.
- [41] Shi WM. Study on connecting method and seismic performance of reinforced and reconstructed beam and column joints. Xi'an university of science and technology; 2011. (in Chinese).
- [42] Park R, Paulay T. Reinforced concrete structures. Boston: Wiley & Sons; 1975.
- [43] JGJ/T101. Specification for seismic test of buildings, Beijing. 2015. (in Chinese).
- [44] GB 50010. Code for design of concrete structures. Beijing: China Architecture and Building Press; 2010. (in Chinese).
- [45] Borosnyói A. Serviceability of CFRP prestressed concrete beams PhD thesis Faculty of Civil Engineering Budapest University of Technology and Economics; 2002.
- [46] Achillides Z, Pilakoutas K. Bond behavior of fiber reinforced polymer bars under direct pullout conditions. *J Compos Constr* 2004;8(2):173–81.